Vesicle dynamics in a confined Poiseuille flow: From steady state to chaos

Othmane Aouane,[1,2,3] Marine Thiébaud,[2] Abdelilah Benyoussef,[3] Christian Wagner,[1] and Chaouqi Misbah[2,*]

[1]*Department of Experimental Physics, Saarland University, 66123 Saarbrücken, Germany*

[2]*Université Grenoble Alpes, LIPHY, F-38000 Grenoble, France*

[3]*LMPHE, URAC 12, Faculté des Sciences, Université Mohammed V—Agdal, Rabat, Morocco*

(Received 31 July 2014; published 18 September 2014)

Red blood cells (RBCs) are the major component of blood, and the flow of blood is dictated by that of RBCs. We employ vesicles, which consist of closed bilayer membranes enclosing a fluid, as a model system to study the behavior of RBCs under a confined Poiseuille flow. We extensively explore two main parameters: (i) the degree of confinement of vesicles within the channel and (ii) the flow strength. Rich and complex dynamics for vesicles are revealed, ranging from steady-state shapes (in the form of parachute and slipper shapes) to chaotic dynamics of shape. Chaos occurs through a cascade of multiple periodic oscillations of the vesicle shape. We summarize our results in a phase diagram in the parameter plane (degree of confinement and flow strength). This finding highlights the level of complexity of a flowing vesicle in the small Reynolds number where the flow is laminar in the absence of vesicles and can be rendered turbulent due to elasticity of vesicles.

DOI: 10.1103/PhysRevE.90.033011 PACS number(s): 47.52.+j, 83.80.Lz, 47.11.Hj

I. INTRODUCTION

Nowadays, vesicles are extensively used as a model for understanding dynamics and deformation of red blood cells (RBCs) at the individual level but also regarding collective phenomena and rheology. Vesicle membranes withstand bending but do not have a shear resistance, unlike RBCs, but they still share several dynamical properties with RBCs, like tank treading and tumbling under linear shear flow, or parachute and slipper shapes under Poiseuille flow [1–3].

Under a Poiseuille flow, the situation of interest in this paper, it is known experimentally that RBCs exhibit a parachute as well a slipper shape [4–7]. Secomb and Skalak [8] have presented a model for the slipper shape based on a lubrication approximation. The slipper shape was also later observed in numerical simulations by Pozrikidis [9]. These authors used a capsule as a model for a RBC. Capsules are shells made of polymers and are endowed with elastic properties, namely, the shear elasticity that mimics the RBC cytoskeleton, i.e., the spectrin network lying underneath the cell membrane. More recently, the minimal ingredients for the occurrence of a slipper shape were identified [10]: a two-dimensional (2D) vesicle even in an unbounded Poiseuille flow exhibits a slipper solution when the flow strength is comparable to that in the microvasculature. The slipper solution occurs as a result of loss of stability of the symmetric solution (also called a parachute). These shapes were further investigated by including the effect of quasirigid bounding walls [11]. This study revealed a large variety of shapes and dynamics such as centered and off-centered periodic oscillations (called snaking). These oscillations are regular and stable in time. Subsequent study in three dimensions has also reported on similar phenomena [12,13]. The present study is a follow-up study to that of Kaoui *et al.* [11] and reveals a variety of new states. For example, we find that vesicles can first undergo snaking (periodic oscillation of the shape in the form of a snake motion) and suddenly undergo a new bifurcation showing period doubling of the temporal oscillation upon variation of a control parameter (e.g., degree of confinement). On further variation of the control parameter the system undergoes a subharmonic cascade oscillation before transitioning to chaos. Scenarios other than period doubling can also occur, as we shall show. We investigate the occurrence of chaos using tools of dynamical systems. We present a full phase diagram in parameter space showing a variety of dynamics.

II. THEORETICAL FRAMEWORK

A. Membrane model

Vesicles in which we are interested consist of a closed bilayer fluid membrane. Typically, vesicle diameters range from a few hundred nanometers to a few hundred micrometers, whereas the thickness of the bilayer is around a few nanometers. At room temperature, bilayer membranes may be regarded as two-dimensional fluids, but one should keep in mind that they may present other phases (e.g., crystal and solid or gel phases) depending on the temperature and the chemical nature of the lipids. The membrane is a two-dimensional incompressible fluid, and therefore its area is locally conserved. Due to membrane impermeability, the volume of the enclosed liquid inside the vesicle is also conserved. Fluid membranes present a viscous resistance to shear stress, leading to a deformation of the membrane with no storage of elastic energy. The only energetic contribution comes from the bending energy. Here we employ the Helfrich elasticity theory for bilayer membranes to describe the curvature energy in two dimensions [14] (2D models have been proven to capture the essential features of vesicles under flow and will be adopted here):

$$\mathcal{H} = \frac{\kappa}{2}\oint (c - c_0)^2 ds, \tag{1}$$

where c and c_0 are, respectively, the mean and spontaneous curvatures; κ is the curvature elastic modulus; s denotes the curvilinear coordinate along the membrane; and $\oint$ refers to an integral over the (2D) membrane contour. In two dimensions the Gaussian curvature is irrelevant owing to the property $\oint c ds = 2\pi$ (an irrelevant constant). A tensionlike energy

*chaouqi.misbah@ujf-grenoble.fr

is added to the bending energy Eq. (1) in order to fulfill the vesicle local perimeter conservation constraint:

$$E_{\text{tens}} = \oint \zeta(s) ds, \tag{2}$$

where ζ is a Lagrange multiplier that enforces constant local length. The force is obtained from the functional derivative of the Hamiltonian, including the tension energy, with respect to the membrane elementary displacement [15]:

$$\mathbf{F}_{\text{mem}} = \kappa \left[\frac{\partial^2 c}{\partial s^2} + \frac{c^3}{2} \right] \mathbf{n} - c\zeta \mathbf{n} + \frac{\partial \zeta}{\partial s} \mathbf{t}, \tag{3}$$

where $\mathbf{n}$ and $\mathbf{t}$ are the normal and tangent unit vectors, respectively. The vesicle is characterized by a reduced area (τ), combining the actual fluid area enclosed by the vesicle contour ($S = \pi R_0^2$) and the area of a disk having the same perimeter as the vesicle with

$$\tau = \frac{2\sqrt{S\pi}}{P} \tag{4}$$

and a viscosity contrast (λ) which expresses the ratio between the inner (η_{in}) and outer (η_{out}) fluid viscosities:

$$\lambda = \frac{\eta_{\text{in}}}{\eta_{\text{out}}}. \tag{5}$$

The effective radius of the cell ($R_0 \equiv \sqrt{S/\pi}$) and the outer viscosity (η_{out}) are chosen to be the characteristic length and viscosity scales, respectively.

B. Boundary integral formulation

The boundary integral method for low Reynolds number flow is well established [16], and we have used it in different contexts in two and three dimensions [10,13,15,17–20]. Here we shall use a special Green's function introduced quite recently in [20] that automatically satisfies the no-slip boundary condition at the bounding walls. Using this special Green's function the velocity along the membrane is given by [20]

$$\frac{1+\lambda}{2}\mathbf{v}(\mathbf{X}) = \mathbf{v}^{\infty}(\mathbf{X}) + \frac{1}{\eta_{\text{out}}} \int_{\gamma} \mathbf{G}_w(\mathbf{X}-\mathbf{X}_0)\mathbf{F}_{\text{mem}}(\mathbf{X}_0) ds(\mathbf{X}_0) + (1-\lambda) \int_{\gamma} \mathbf{v}(\mathbf{X}_0)\mathbf{K}_w(\mathbf{X}-\mathbf{X}_0)\mathbf{n}(\mathbf{X}_0) ds(\mathbf{X}_0), \tag{6}$$

where $\mathbf{X}$ and $\mathbf{X}_0$ are two position vectors belonging to the membrane (γ). $\mathbf{v}$ and $\mathbf{v}^{\infty}$ are the membrane's velocity and the imposed velocity. $\mathbf{G}_w$ and $\mathbf{K}_w$ stand for the Green's-function second- and third-order tensors for two parallel walls, and $\mathbf{v}^{\infty}(\mathbf{X})$ is the imposed Poiseuille flow (to be specified below). The detailed expression of the Green's functions is given in [20]. Because of the use of this special Green's function the integral is only performed along the vesicle, and not along the bounding walls. This provides us with a quite powerful technique, as recently demonstrated [20,21]. The boundary conditions used in order to derive the integral equation (6) are (i) a no-slip condition at the walls and at the membrane, (ii) stress balance at the membrane, and (iii) membrane inextensibility.

The external flow and confinement introduce two additional dimensionless numbers: the so-called capillary number (C_k) to quantify the flow strength over bending forces and the confinement (C_n) to describe the ratio between the effective diameter of the vesicle and the width of the channel. The imposed Poiseuille flow is written as

$$\begin{cases} v_x^{\infty} = v_{\max}\left[1 - \left(\frac{y}{W/2}\right)^2\right] \\ v_y{}^{\infty} = 0. \end{cases} \tag{7}$$

The capillary number is defined as

$$C_k = \frac{\eta_{\text{out}} R_0^4}{\kappa} \frac{v_{\max}}{(W/2)^2} \equiv \tau_c \dot{\gamma}, \tag{8}$$

and the confinement is written as

$$C_n = \frac{2R_0}{W}, \tag{9}$$

where R_0, W, and $v_{\max}$ are the effective radius of the cell, the width of the channel, and the maximum velocity of the unperturbed Poiseuille flow. We define the characteristic shear rate $\dot{\gamma}$ as the imposed velocity gradient evaluated at $y = R_0/2$ and equal to $R_0 v_{\max}/(W/2)^2$, and $\tau_c = \eta_0 R_0^3/\kappa$ is the characteristic shape relaxation time. Time will be measured hereafter in units of τ_c, and distances will be measured in units of R_0. The details of numerical treatments are similar to those used in [19,22].

III. RESULTS AND DISCUSSION

We performed a systematic scan in the three-dimensional parameter space (λ, C_k, C_n), in order to explore the various intricate behaviors of a vesicle under a Poiseuille flow. Instead of C_k we shall use the combination $C_k W/R_0 = C_k/2C_n$, which corresponds to the definition of the capillary number from [11,23]. This will simplify comparison with the results of [23]. In all simulations, we have set the reduced area τ to 0.6, which is close to that of a RBC in two dimensions.

A. Effect of flow strength and confinement on the shape of a vesicle (case $\lambda = 1$)

We first set the viscosity contrast to $\lambda = 1$ and explored the effect of the confinement and the capillary number on the morphology of the cell. In order to test the new code based on the Green's function that vanishes at the wall [20], we have first confirmed the previously reported results [11,23], namely, the existence of six different states: parachutelike shape, confined and unconfined slipperlike shapes, centered and off-centered oscillating motions (called snaking in [11]), and peanutlike shape [23]). Figure 1 shows the parachutelike and confined slipperlike solutions. The snaking motions (centered and noncentered) recently reported by Kaoui *et al.* [11] and Tahiri *et al.* [23] have not exhausted all intricate dynamics. By investigating the evolution of solutions under close scrutiny we have discovered a variety of new states ranging from simple oscillations to complex multiperiodic oscillations, until chaotic motion prevails, as described below.

1. Transition to chaos via a subharmonic cascade

We have set $C_k W/R_0 = 5$ and varied the degree of confinement C_n. The results are shown in Fig. 2, where we represent

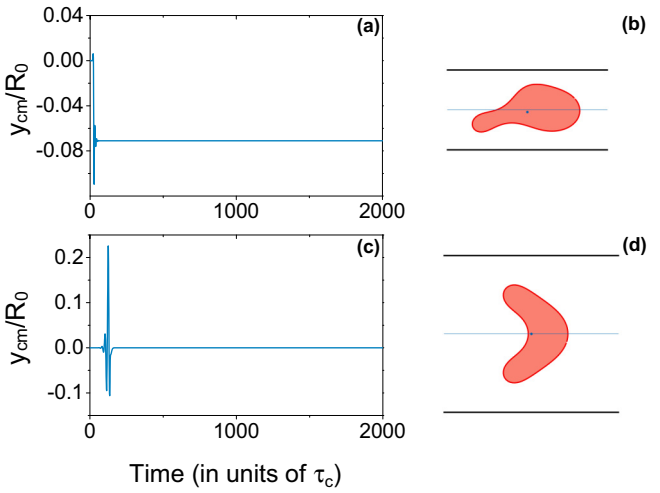

FIG. 1. (Color online) Stationary shape and history of the center of mass vertical position as a function of time. (a and b) Slipper solution ($C_k W/R_0 = 6.25$ and $C_n = 0.8$). (c and d) Parachute solution ($C_k W/R_0 = 6.25$ and $C_n = 0.44$). The x axis codes are shown for the lateral position of the mass center y_{CM} of the cell scaled by the effective radius of the cell (R_0).

the vertical position of the vesicle center of mass (y_{CM}) as a function of time. Below a first critical value of C_n, the slipper becomes unstable in favor of a snaking motion (off-centered). This is a Hopf bifurcation. Close to the bifurcation point the temporal evolution of the amplitude of lateral excursion of the center of mass (y_{CM}) remains constant over time [see Fig. 2(b)]. By further reducing C_n, the simple snaking solution undergoes a new bifurcation whereby the period of oscillation has doubled [Fig. 2(c)] and then quadrupled for a smaller value of C_n [Fig. 2(d)]. By further decreasing C_n, dynamics enter a chaotic regime (Fig. 3). In Fig. 4, we represent the amplitude A of excursion of the center of mass in the y

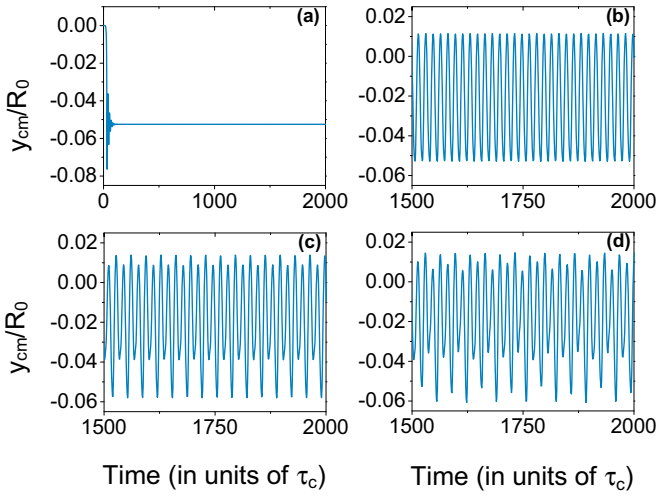

FIG. 2. (Color online) The center of mass vertical position as a function of time. (a) Slipper solution ($C_k W/R_0 = 5$ and $C_n = 0.769$). (b) Snaking dynamics ($C_k W/R_0 = 5$ and $C_n = 0.733$). (c) Period-doubling dynamics ($C_k W/R_0 = 5$ and $C_n = 0.729$). (d) Period-quadrupling dynamics ($C_k W/R_0 = 5$ and $C_n = 0.727$).

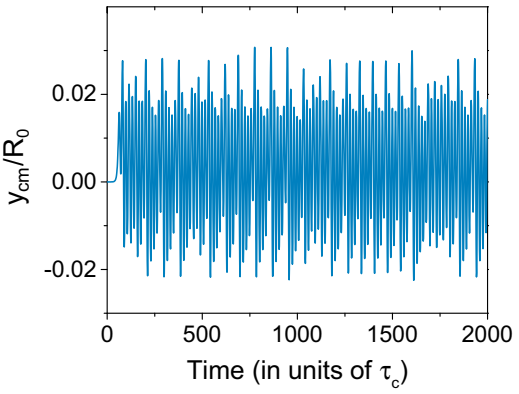

FIG. 3. (Color online) The center of mass vertical position as a function of time. An apparently chaotic regime is found for $C_k W/R_0 = 5$ and $C_n = 0.689$.

direction (that is the absolute value of the difference between two successive maxima). Since a slipper (as well as a parachute solution) moves along a line in the x direction (see Fig. 1) the amplitude of lateral excursion is zero above a critical value of $C_n = 0.75$ (Fig. 4). Figure 4 shows the amplitude as a function of C_n, where we can see the beginning of a subharmonic cascade, and the signature of accumulation of bifurcation points. This is a universal behavior, well documented in chaos textbooks [24–26]. The subharmonic cascade is one of the three generic scenarios of transition to chaos (the two others being intermittency and quasiperiodicity). Here we have represented only the main oscillation (period 1), the period doubling (period 2), and the period quadrupling (period 4). Because of the universal accumulation in the subharmonic cascade (that is, the location points of new bifurcations to higher-order oscillations become closer and closer), the transition to periods 8 and 16, for example, requires tuning very carefully the control parameter as well as increasing numerical precision (a significant reduction of the numerical mesh size leads to excessive computation time), and it was not our aim to provide a very detailed analysis of the higher-order period-doubling cascade. Starting from the regime of period-4

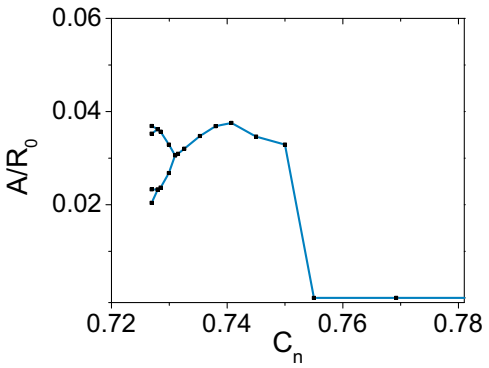

FIG. 4. (Color online) Period-doubling bifurcation diagram. The capillary number is fixed ($C_k W/R_0 = 5$), and only the confinement C_n is changed. The x and y axes stand for the confinement and the amplitude of the oscillations, respectively.

oscillation, we found that a quite small variation of C_n (of about 4%) leads to chaos, as shown in Fig. 3.

2. *Transition to chaos via a period-tripling bifurcation*

The subharmonic cascade is one of the three classical scenarios of transition to chaos (in addition to intermittency and quasiperiodicity). The subharmonic cascade corresponds to a cascade where at each bifurcation point the period is doubled (or the frequency is halved). By analyzing the dynamics of the initial snaking motion in other regions of parameter space, we have discovered that the snaking motion can also lose its stability in favor of a period-tripling bifurcation, which is a less-known scenario as compared to the period-doubling one. We show in Fig. 5 both a typical temporal signal and the bifurcation diagram. Period-tripling bifurcations and more complex transitions were also reported in literature. We take as a reference, for instance, the pioneering paper of Li and Yorke [27], where they introduced the first mathematical definition of discrete chaos, showing the relation between period 3 and chaos. Lui [28] presented sufficient mathematical conditions for period-tripling and period-n bifurcations. Ze-Hui *et al.* [29] reported subharmonic bifurcations in a granular system, in the sequence of period tripling, period sextupling, and chaos. Zhusubaliyev and Mosekilde [30] showed transition from periodic to chaotic oscillations through period-doubling, -tripling, -quadrupling, and -quintupling bifurcations, among others. They also discussed more complex transitions, from a family of cycles to another family of cycles with multiple periods.

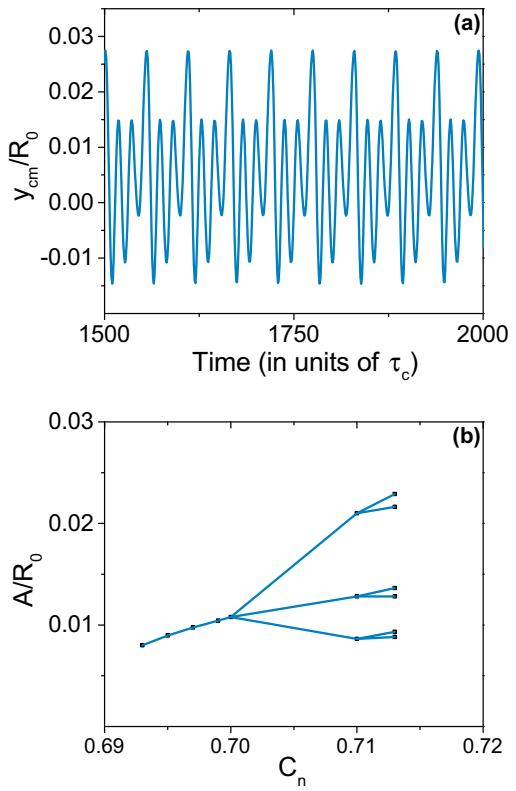

FIG. 5. (Color online) Period-tripling motion of the mass center. (a) Temporal behavior for a period-tripling dynamics ($C_kW/R_0 = 4.611$ and $C_n = 0.71$). (b) Bifurcation diagram ($C_kW/R_0 = 4.611$).

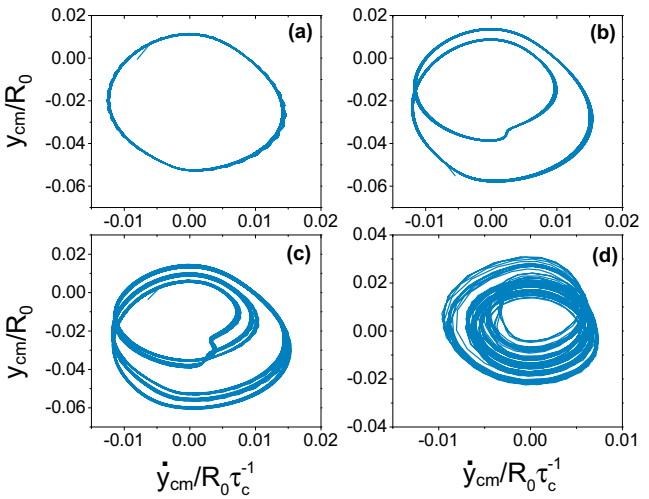

FIG. 6. (Color online) Poincaré sections of different oscillations observed by decreasing the confinement when the capillary number C_kW/R_0 has been fixed at 5. The y axis stands for the y component of the mass center of the cell, and the x axis stands for its derivative with respect to time. (a) $C_n = 0.733$. (b) $C_n = 0.729$. (c) $C_n = 0.727$. (d) $C_n = 0.689$.

3. *Transition to chaos*

In order to characterize chaotic dynamics we have performed a Poincaré map as well as Fourier transforms of the temporal evolution of center of mass amplitude. Figure 6 displays the Poincaré sections relative to the different 1, 2, and 4 periodic oscillations, in addition to the chaotic one. In this case, the gradual decrease of the confinement under a low capillary number ($C_kW/R_0 = 5$ in these simulations) is responsible for the observed transitions. The motion actually can be assimilated to a flagellalike motion, where the vesicle undergoes a periodic or a chaotic up-down motion. Snapshots of this motion are shown in Fig. 7 [31]. Figure 8 shows the Fourier spectrum of different dynamics. We see there the occurrence of the cascade until the transition to chaos.

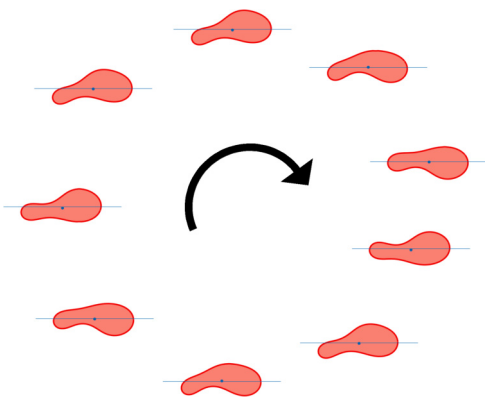

FIG. 7. (Color online) Snapshots of a cycle of period-doubling dynamics ($C_kW/R_0 = 5$ and $C_n = 0.729$). The cell seems to move like a spermatozoon, using its tail as a flagellum. The straight solid blue line indicates the centerline of the channel, and the blue point indicates the mass center of the cell.

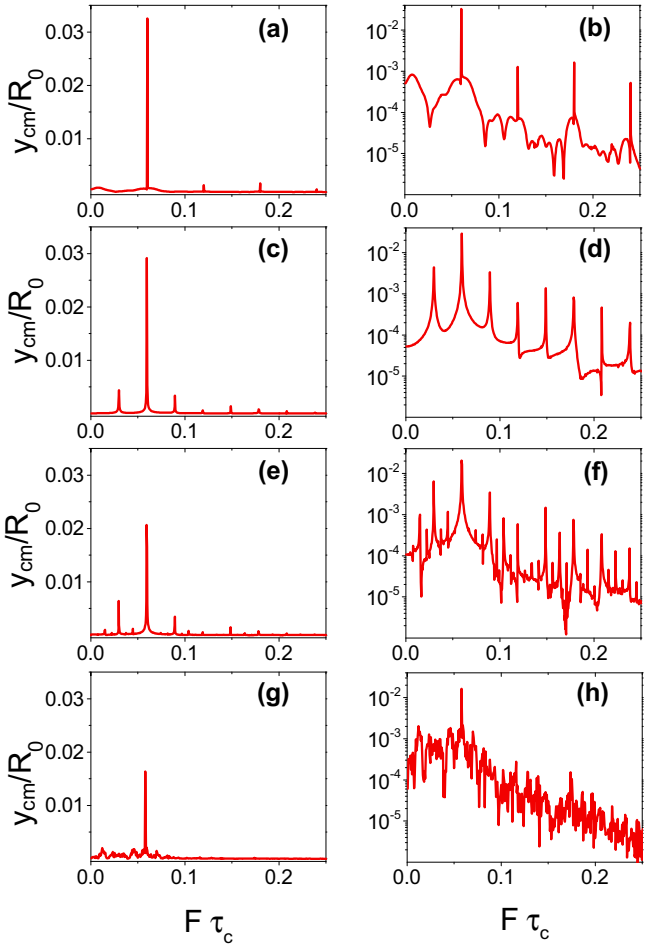

FIG. 8. (Color online) Fourier spectrum of different dynamics in linear (a, c, e, and g) and semi-logarithmic (b, d, f, and h) coordinates: (a and b) Snaking dynamics ($C_k W/R_0 = 5$ and $C_n = 0.733$). (c and d) Period-doubling dynamics ($C_k W/R_0 = 5$ and $C_n = 0.729$). (e and f) Period-quadrupling dynamics ($C_k W/R_0 = 5$ and $C_n = 0.727$). (g and h) Chaotic dynamics ($C_k W/R_0 = 5$ and $C_n = 0.689$). The semi-logarithmic scale allows one to see more easily the continuum spectrum characteristic of chaotic regimes. The x axis codes are shown for the frequency F scaled by the characteristic time τ_c.

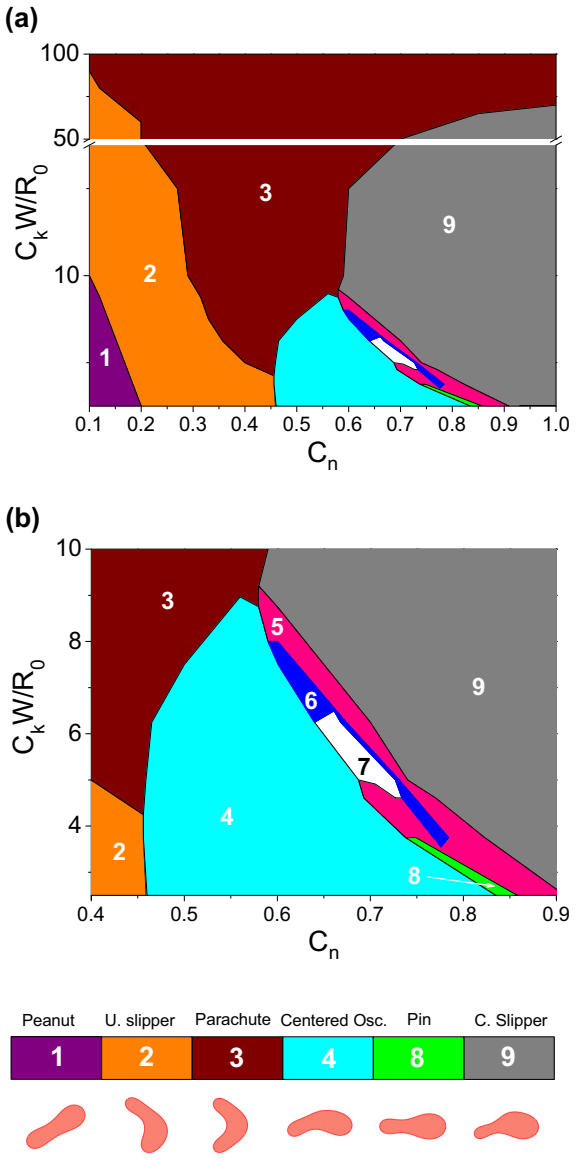

FIG. 9. (Color online) Phase diagram summarizing the different morphologies and dynamics of a single vesicle with a viscosity contrast set to unity ($\lambda = 1$). (a) Overview of the phase diagram. (b) Zoom on the region where oscillations occur. The combined effect of the confinement and flow strength leads to nine distinct regions represented by different colors in the phase diagram: peanutlike shape (purple), unconfined slipperlike shape (orange), parachutelike shape (dark red), confined slipperlike shape (gray), centered oscillations (cyan), multiple periodic oscillations (dark blue), chaotic oscillations (white), off-centered oscillations (pink), and pinlike shape (green). Note that three regions are not represented in the legend, namely, the multiple periodic, chaotic, and off-centered oscillations.

B. Phase diagram

We have performed a systematic analysis in order to determine the region of different dynamical manifestation going from order to chaos. The results are shown in Fig. 9. Besides the dynamics and shapes reported earlier [11,23], revealing slipper, parachute, and snaking, we have identified here more complex dynamics, going from higher-order oscillatory motion to chaos. Surprisingly enough, a simple situation treated here, namely, a 2D vesicle under a Poiseuille flow, has revealed broadly nine different kinds of motion (actually the number is even larger, since in Fig. 9 we do not specify the kind of multiple oscillation). This result highlights the complexity of this free boundary problem, where membrane elasticity that acts here only via bending forces can trigger rich dynamics.

C. RBC-like vesicles in microcirculation conditions

The complex dynamics discussed above occur at low enough flow strength. We will examine now what happens at large enough flow strength by exploring other viscosity contrasts. We will start our study by fixing the viscosity ratio to $\lambda = 5$ (equivalent to a cytoplasmic viscosity of around 5 cP), which corresponds to the one of a young red blood

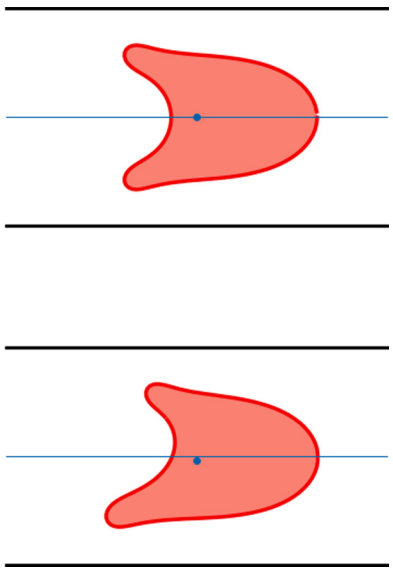

FIG. 10. (Color online) Stationary shapes exhibited by a RBC-like vesicle under the same conditions of flow and confinement ($C_k = 120$ and $C_n = 0.7$): $\lambda = 5$, cytoplasmic viscosity ≈5 cP (top) and $\lambda = 10$, cytoplasmic viscosity ≈10 cP (bottom).

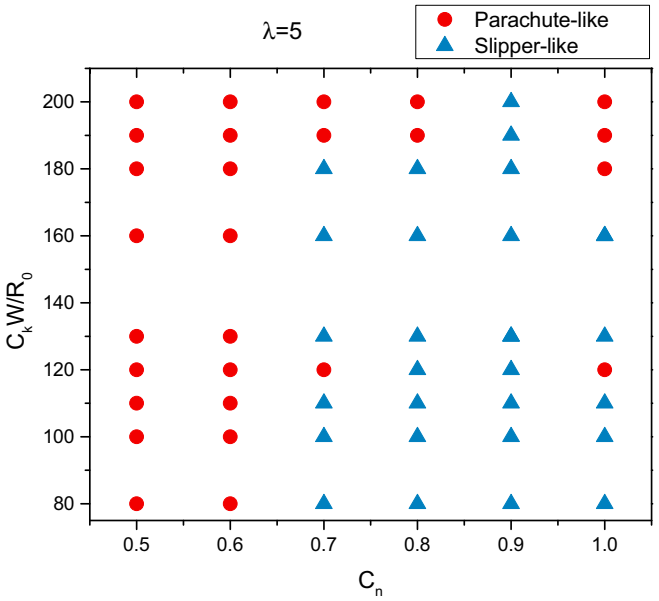

FIG. 11. (Color online) Phase diagram of a red blood cell-like vesicle ($\lambda = 5$) in a Poiseuille flow showing the existence of three different regimes at very high capillary number.

cell. Recently Tahiri *et al.* [23] investigated numerically the deformation of a single vesicle bounded by two quasirigid walls (walls could deform slightly) using a boundary integral formulation in two dimensions. They reported, in addition to the symmetric and asymmetric regions, on a region of parameter space where there is a coexistence between the symmetric and asymmetric shapes (parachute and slipper). We have reinvestigated the effect of both confinement and capillary number on the morphology of a single vesicle for the case of rigid walls. We have observed two possible solutions for the range of parameters investigated, namely, (i) parachutelike shapes and (ii) slipperlike shapes (Fig. 10). We have summarized the results in a phase diagram in Fig. 11. Similar behavior was reported experimentally and discussed in [5]. We restrict the use of the word *parachute* to the strictly symmetrical solutions, where the word *slipper* covers the asymmetrical solutions. We have found series of symmetric-asymmetric-symmetric transitions. This transition was also observed in the experimental work of Abkarian *et al.* [6] and Tomaiuolo *et al.* [7], but not discussed in detail. Tahiri *et al.* [23] report that a change in the inner viscosity of the cell from around 1 cP (viscosity of the plasma) to around 5 cP (a typical value for a young red blood cell) leads to different stationary shapes. Given the importance of this parameter we have also investigated another larger value. It is important first to underline that (i) the cytoplasmic viscosity of the red blood cell is a variable from one cell to the other (within the same organism), due to age, and then (ii) its value depends on the mean corpuscular hemoglobin concentration (MCHC). The MCHC describes the concentration of the hemoglobin per unit volume of a red blood cell. Cokelet and Meiselman report that the value of the cytoplasmic viscosity increases in a nonlinear manner with the MCHC [32]. During its lifespan, the mean cell volume and the mean surface area of the red blood cell decrease with a constant ratio: the reduced volume of the cell remains the same [33,34]. Since the concentration of the hemoglobin stays constant over time, the MCHC increases as a function of the age of the cell. A typical value of the cytoplasmic viscosity for a young red blood cell is around 5–7 cP and corresponds to a value of MCHC of about $32g/dl$ [34,35]. For MCHC around $40g/dl$, the viscosity of the cell nearly quadruples [36]. Therefore, one natural question is the impact of the cytoplasmic viscosity of the red blood cell on dynamics. We would like to see how the phase diagram changes (at high enough flow strength, corresponding to physiological values) when the viscosity contrast is high enough as compared to the so-called normal one, $\lambda = 5$. We have set $\lambda = 10$, which corresponds to a cytoplasmic viscosity of around 10 cP. We report the results in Fig. 12. We observe that the slipperlike solution prevails when increasing the confinement and disappears for $C_k W/R_0 \geqslant 190$. The separation region between the symmetric and asymmetric solutions is more pronounced than for the case of $\lambda = 5$. Indeed, for the range of the explored data, we do not observe any kind of transition from symmetry to asymmetry to symmetry (as for $\lambda = 5$), but rather we observe a transition from symmetric to asymmetric shapes. We show clearly that the stationary solutions are sensitive to inner viscosity changes, as shown in Fig. 10. Considering that in most of the experimental works the cytoplasmic viscosity of the red blood cells is an unknown variable and most probably a nonuniform one, this may give a lead about why, for fixed flow and confinement conditions, symmetric and asymmetric shapes can both be observed. Our study regarding this effect is only indicative, and a systematic analysis should be postponed.

IV. CONCLUDING REMARKS

The most pronounced result of our study is the discovery of surprisingly complex behavior of vesicles in a Poiseuille flow. The dynamics has revealed nine major distinct shapes

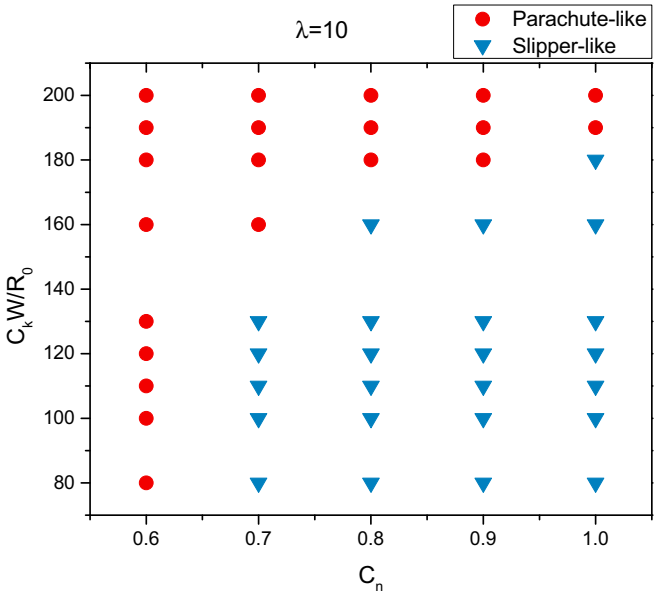

FIG. 12. (Color online) Phase diagram for $\lambda = 10$. The red and blue dots indicate, respectively, parachutelike and slipperlike shapes.

and dynamics, ranging from symmetric and nonsymmetric solutions up to chaos. Dynamics of vesicles are treated here in the Stokes regime. In the absence of inertia, it is a classical result that the Poiseuille flow is always laminar. The existence of a single elastic object within the flow, acting only via bending forces, completely destroys the overall picture: chaotic dynamics take place. It would be interesting to investigate in the future the behavior of these chaotic regimes in the presence of many vesicles. It is tempting to conjecture that the composite fluid would look chaotic not only in time (as reported here) but also in space. This problem could be viewed as a class of systems exhibiting the so-called elastic turbulence [37], that is a turbulence caused by the elasticity of the suspending entities when coupled to fluid flow in the purely Stokes regime. Elastic turbulence is characterized by a cascade of transfer of energy from large to small scales, akin to the Kolmogorov cascade for classical turbulence. A systematic analysis should be undertaken before drawing conclusive answers.

In a two-dimensional unbounded Poiseuille flow, the shape diagram of vesicles shows centered symmetric (parachute and bullet) shapes and off-centered asymmetric (slipper) shapes [10]. These results are also observed in three-dimensional simulations [13]. Snaking oscillations are observed in both two-dimensional [11] and three-dimensional [12] simulations of vesicles in a confined Poiseuille flow. Chaotic dynamics, which were not reported in the previous numerical studies, were observed here under a close scrutiny. It is likely that the kind of solutions reported in this study should also occur in three dimensions with a rigorous investigation. To the limits of the authors' knowledge, there are no results in two dimensions that have not been confirmed in three dimensions. For all these reasons, it would be desirable to extend this work in three dimensions.

We hope that this study will trigger further investigations both numerically and experimentally.

ACKNOWLEDGMENTS

We acknowledge many fruitful discussions with Dr. G. Ghigliotti at University of Nice Sophia Antipolis and Dr. A. Farutin at University Grenoble Alpes. This work was supported by the German Science Foundation research initiative Grant No. SFB1027 and the graduate school GRK Grant No. 1276, by Deutsch-Französische Hochschule (Université Franco-Allemande) (the German-French University). M.T. and C.M. acknowledge financial support from Centre National d'Etudes Spatiales and European Space Agency.

[1] M. Abkarian and A. Viallat, Soft Matter **4**, 653 (2008).
[2] P. M. Vlahovska, T. Podgorski, and C. Misbah, C. R. Phys. **10**, 775 (2009).
[3] P. M. Vlahovska, D. Barthes-Biesel, and C. Misbah, C. R. Phys. **14**, 451 (2013).
[4] R. Skalak and P. I. Branemark, Science **164**, 717 (1969).
[5] H. Schmid-Schönbein and P. Gaehtgens, Scand. J. Clin. Lab. Invest. **41**, 13 (1981).
[6] M. Abkarian, M. Faivre, R. Horton, K. Smistrup, C. A. Best-Popescu, and H. A. Stone, Biomed. Mater. **3**, 034011 (2008).
[7] G. Tomaiuolo, M. Simeone, V. Martinelli, B. Rotoli, and S. Guido, Soft Matter **5**, 3736 (2009).
[8] T. Secomb and R. Skalak, Microvasc. Res. **24**, 194 (1982).
[9] C. Pozrikidis, Ann. Biomed. Eng. **33**, 165 (2005).
[10] B. Kaoui, G. Biros, and C. Misbah, Phys. Rev. Lett. **103**, 188101 (2009).
[11] B. Kaoui, N. Tahiri, T. Biben, H. Ez-Zahraouy, A. Benyoussef, G. Biros, and C. Misbah, Phys. Rev. E **84**, 041906 (2011).
[12] D. A. Fedosov, M. Peltomaki, and G. Gompper, Soft Matter **10**, 4258 (2014).
[13] A. Farutin and C. Misbah, Phys. Rev. E **89**, 042709 (2014).
[14] W. Helfrich, Z. Naturforsch. **28**, 693 (1973).
[15] B. Kaoui, G. H. Ristow, I. Cantat, C. Misbah, and W. Zimmermann, Phys. Rev. E **77**, 021903 (2008).
[16] C. Pozrikidis, *Boundary Integrals and Singularity Methods for Linearized Viscous Flow* (Cambridge University Press, Cambridge, 1992).
[17] I. Cantat and C. Misbah, Phys. Rev. Lett. **83**, 880 (1999).
[18] H. Selmi, L. Elasmi, G. Ghigliotti, and C. Misbah, Discrete Cont. Dyn. Syst. Ser. B **15**, 1065 (2011).
[19] T. Biben, A. Farutin, and C. Misbah, Phys. Rev. E **83**, 031921 (2011).
[20] M. Thiébaud and C. Misbah, Phys. Rev. E **88**, 062707 (2013).
[21] M. Thiébaud, Z. Shen, J. Harting, and C. Misbah, Phys. Rev. Lett. **112**, 238304 (2014).
[22] G. Ghigliotti, T. Biben, and C. Misbah, J. Fluid Mech. **653**, 489 (2010).
[23] N. Tahiri, T. Biben, H. Ez-Zahraouy, A. Benyoussef, and C. Misbah, Microvasc. Res. **85**, 40 (2013).

[24] M. Schroeder, *Fractals, Chaos, Power Laws: Minutes from an Infinite Paradise* (Dover, New York, 2012).
[25] E. Ott, *Chaos in Dynamical Systems* (Cambridge University Press, Cambridge, 2002).
[26] P. Bergé, Y. Pomeau, and C. Vidal, *L'Ordre dans le Chaos* (Hermann, Paris, 1992).
[27] T.-Y. Li and J. A. Yorke, Am. Math. Mon. **82**, 985 (1975).
[28] S. Lui, J. Mod. Math. Front. **2**, 74 (2013).
[29] J. Ze-Hui, W. Yun-Ying, and W. Jing, Europhys. Lett. **74**, 417 (2006).
[30] Z. Zhusubaliyev and E. Mosekilde, *Bifurcations and Chaos in Piecewise-Smooth Dynamical Systems*, World Scientific Series on Nonlinear Science: Monographs and Treatises, Vol. 44 (World Scientific, Singapore, 2003).
[31] See Supplemental Material at http://link.aps.org/supplemental/10.1103/PhysRevE.90.033011 for the different dynamics.
[32] G. R. Cokelet and H. J. Meiselman, Science **162**, 275 (1968).
[33] O. Linderkamp and H. J. Meiselman, Blood **59**, 1121 (1982).
[34] S. Guido and G. Tomaiuolo, C. R. Phys. **10**, 751 (2009).
[35] N. Mohandas and P. G. Gallagher, Blood **112**, 3939 (2008).
[36] S. Chien, Annu. Rev. Physiol. **49**, 177 (1987).
[37] A. Groisman and V. Steinberg, Nature (London) **405**, 53 (2000).